Changing Ozone Sensitivity in the South Coast Air Basin during the COVID-19 Period

Jason R. Schroeder[1], Chenxia Cai[1], Jin Xu[1], David Ridley[1], Jin Lu[1], Nancy Bui[1], Fang Yan[1,*], Jeremy Avise[1]

[1] California Air Resources Board, 1001 I Street, Sacramento, CA, USA

[*] Now at ICF Consulting, 980 9th Street, Sacramento, CA, USA

Correspondence to: Jason R. Schroeder (Jason.schroeder@arb.ca.gov)

Abstract. The South Coast Air Basin (SoCAB), which includes the city of Los Angeles and is home to more than 15 million people, frequently experiences ozone (O_3) levels that exceed ambient air quality standards. While strict regulation of O_3 precursors has dramatically improved air quality over the past fifty years, the region has seen limited improvement in O_3 over the past decade despite continued reductions in precursor emissions. One contributing factor to the recent lack of improvement is a gradual transition of the underlying photochemical environment from a VOC-limited regime towards a NO_x-limited one. The changes in human activity prompted by COVID-related precautions in Spring and Summer of 2020 exacerbated these already-occuring changes in the O_3 precursor environment. Analyses of sector-wide changes in activity indicate that emissions of NO_x decreased by 15-20% during Spring (April – May) and 5-10% during Summer (June – July) relative to expected emissions for 2020, largely due to changes in mobile source activity. Historical trend analysis from two indicators of O_3 sensitivity (the satellite $HCHO/NO_2$ ratio and the O_3 weekend/weekday ratio) revealed that Spring of 2020 was the first year on record to be on average NO_x-limited, while the "transitional" character of recent Summers became NOx-limited due to COVID-related NO_x reductions in 2020. Model simulations performed with base-case and COVID-adjusted emissions capture this change to a NO_x-limited environment and suggest that COVID-related emissions reductions were responsible for a 0-2 ppb decrease in O_3 over the study period. Reaching NO_x-limited territory is an important regulatory milestone, and this study suggests that deep reductions in NO_x emissions (in excess of those observed in this study) would be an effective pathway for long-term O_3 reductions.

1 Introduction

The South Coast Air Basin (SoCAB), which is home to the city of Los Angeles and more than 15 million people, has experienced steadily decreasing levels criteria pollutants such as ozone (O_3) over the past few decades. However, recent years have been characterized by basin-wide O_3 levels that have been flat or even increasing (Aqmd, 2016). Recent literature has suggested that this trend is the result of non-linear changes in the underlying chemistry that creates O_3 in the SoCAB (Pollack et al., 2013; Fujita et al., 2013). Therefore, efforts to reduce O_3 in the SoCAB need to understand and account for these non-

30   linearities in the ozone photochemistry and how the photochemical state may change over time as emissions are further reduced (Fujita et al., 2016). In this work, we explore how the photochemical state of the SoCAB changed as a result of the emissions reductions associated with society's response to COVID-19, which resulted in reduced mobile source emissions. This provides a preview of how the photochemical state of the SoCAB may change in the near future, allowing us to better-predict the long-term effectiveness of regulations aimed at reducing O_3.

35   There are no primary emission sources of O_3, and instead it is formed through the photochemical interaction between emissions of volatile organic compounds (VOCs) and nitrogen oxides ($NO_x = NO + NO_2$) (Chameides and Walker, 1973; Chameides et al., 1992). However, O_3 chemistry is complex and varies non-linearly with respect to precursor concentrations. Therefore, a detailed understanding of the sensitivity of local O_3 formation to changes in the precursor environment is essential for drafting effective mitigation strategies. This non-linear response of O_3 to concentrations of its precursors results in the presence of two

40   distinct photochemical regimes, commonly referred to as "NO_x-limited" and "VOC-limited" (Chameides et al., 1992; Kleinman et al., 1997; Sillman et al., 1990). Historically, the O_3 season in the SoCAB has been characterized as VOC-limited due to an overabundance of NO_x, with high NO_x emissions dominated by mobile sources. In such VOC-limited environments, where a significant fraction of the VOCs are from biogenic sources, reduction of NO_x is necessary to achieve long-term ozone reduction but can lead to short-term O_3 increases without concurrent action to reduce VOC emissions. Over the past few

45   decades, reductions in SoCAB NO_x emissions have been accompanied by concurrent reductions in anthropogenic VOC emissions, yielding a general decrease in basin wide O_3 (Aqmd, 2016). In recent years, while concurrent VOC and NO_x reductions have continued, VOC reductions have been outpaced by NO_x reductions, offering one explanation for the recent flattening in the O_3 trend. Given California's recent initiatives to phase out internal combustion engines in light duty and heavy duty vehicles, which would greatly reduce NO_x emissions, a critical question remains: when will the SoCAB become NO_x-

50   limited and begin to experience immediate benefits in the form of reduced O_3 from the reduction in NO_x emissions?
Recent literature has indicated that the SoCAB has been moving away from a VOC-limited environment towards a NO_x-limited environment, but discerning the exact nature of the current photochemical state in this "transitional" environment is challenging due to the limitations of individual observation platforms. Surface monitoring networks can be used for spatiotemporal exploration of trace gases and the weekend/weekday (WE/WD) effect, thus providing insight into the

55   photochemical regime at local scales. The WE/WD effect is a well-studied phenomenon whereby reduced heavy-duty truck activity and emissions on weekends can be employed as a natural experiment to explore the response of O_3 to changes in NO_x emissions. In a VOC-limited environment, weekend O_3 tends to be higher than weekday O_3, and vice-versa for a NO_x-limited environment. However, surface monitoring networks are subject to spatial gaps, incomplete temporal coverage, and only represent conditions at the surface (O_3 production is integrated throughout the planetary boundary layer). Satellite

60   measurements, on the other hand, offer greatly improved spatial coverage with daily viewings. Column-integrated measurements of the $HCHO/NO_2$ ratio have been applied as a coarse indicator of O_3 sensitivity in the lower troposphere, with very low ratios indicative of VOC-limited regimes, and very high ratios indicating NO_x-limited regimes (Martin et al., 2004; Duncan et al., 2010). However, recent studies have shown that this ratio incurs a large degree of uncertainty, and may not be

useful for classifying regimes that are near a "transitional" state (Schroeder et al., 2017). Furthermore, measurements from polar-orbiting satellites are only collected once per day (typically around midday), meaning that satellite measurements are insufficient to explore diurnal trends in O_3 chemistry. Chemical transport models (CTMs) - which include emissions, transport, and chemistry – provide the most robust method of studying O_3 chemistry by allowing users to explore changes in simulated O_3 in response to changes in precursor emissions. However, CTMs are subject to uncertainties in many parameters (particularly emissions), leading to uncertainty in the simulated dependency of O_3 on its chemical precursors. Rather than rely on any one of these approaches, this study uses a multi-perspective approach whereby all three data sources (satellite data, surface monitors, and a CTM) are integrated into our analysis to paint a cohesive picture of the O_3 photochemical regime in the SoCAB during the COVID-19 period.

In the SoCAB, mobile sources are estimated to be responsible for more than three quarters of all NO_x emissions, with heavy-duty trucks comprising the largest sub-sector for mobile source NO_x emissions (CEPAM, 2018). Recent legislature passed by the State of California aims to eliminate new sales of light duty internal combustion engines by 2035 and heavy-duty internal combustion engines by 2040. Given the drastic NO_x reductions expected by these programs, there is considerable interest in classifying the current photochemical state of the SoCAB and understanding when the region may transition to a NO_x-limited environment, thus maximizing the O_3 benefit of these policies. California began implementing a 'stay home' policy in March of 2020 in an effort to combat the spread of COVID-19. As a result of this policy, mobile source activity temporarily dropped in Spring and early Summer of 2020, providing a potential glimpse into how SoCAB O_3 chemistry may look in the near future. Recent literature examining the COVID-19 period has highlighted that the SoCAB experienced a 20-40% decrease in ambient NO_x concentrations, no discernable change in ambient VOC concentrations, and inconsistent changes in O_3 across the basin (Parker et al., 2020; Goldberg et al., 2020; Barletta et al., 2020; Naeger and Murphy, 2020). This work builds upon these studies by using a suite of indicators to derive process-level understanding and establish causal relationships between emissions, photochemical state, ambient concentrations, and meteorology during the COVID-19 period in the SoCAB. We show that the additional NO_x reductions associated with COVID-19 were on average sufficient to shift O_3 chemistry in the basin into a NO_x-limited regime for the first time since observations began. However, changes in chemical regime alone were not enough to reduce ambient O_3 concentrations, especially when coupled with warmer-than-usual temperatures observed during the study period.

2 Methodology

2.1 Quantifying Changes in On-road and Off-road Mobile Source Activity

Although COVID-19 resulted in many behavioral changes among residents of the SoCAB, none had a greater effect on emissions of O_3 precursors than reductions in vehicle activity. This study quantifies the changes in vehicle miles traveled (VMT) using vehicle activity monitoring and tracking data from a suite of publicly available sources to quantify changes due to COVID-related precautions. These data sources include (1) VMT from StreetLight Data, Inc., (Streetlight, 2020) (2) VMT

from Caltrans Performane Measurement System (PeMS) (Caltrans, 2020b), (3) truck counts from Weigh-in-Motion (WIM) stations (Caltrans, 2020a), (4) relative changes of vehicle trips from Geotab, and (5) diesel and gasoline fuel sales from California Department of Tax and Fee Administration (CDTFA).

County-wide data from Streetlight was used to evaluate total VMT trends from March 1, 2020 to the end of July 2020 (Streetlight, 2020). Total VMT is estimated as mean trip length and the total number of trips taken by the full population. To cross-validate Streetlight VMT estimates, VMT from Caltrans' PeMS was computed with data collected in real-time from nearly 40,000 individual detectors spanning the freeway system across all major metropolitan areas of California (Caltrans, 2020b). Though PeMS data is not directly used for emission estimates in this analysis due to its limited vehicle activity coverage (e.g. only highways), it was used to cross-validate Streetlight data. Both datasets showed similar trends of total VMT reduction during the study period. A time series depicting total VMT derived from Streetlight data is shown in Figure S1 in the Supplemental Info.

Heavy-duty trucks are responsible for nearly one third of all mobile source NO_x emissions in the SoCAB, thus special care must be taken to ensure accurate quantification of VMT from heavy-duty vehicles. In this analysis, daily truck counts with Federal Highway Administration (FHWA) Class 4 and above from Weigh-in-Motion (WIM) stations are used as surrogates to reflect the changes of heavy-duty vehicle activity due to COVID-19 shelter-in-place. Electronic sensors at WIM stations capture and record truck counts, as well as their axle and gross vehicle weights, when vehicles drive over a measurement site (Caltrans, 2020a). WIM stations with missing data during critical days of observation were excluded from this study, except for the station the 710 freeway, where the missing data were filled based on the average regional contributions (50%-60% during weekdays and 20%-30% during weekends) and observed total region total. Commercial heavy-duty truck trip trends from Geotab were used to cross check WIM data. Despite that Geotab data is limited by telematics data from commercial fleets they manage, it shows similar pattern to WIM truck counts. A time series showing WIM heavy-duty VMT (HD VMT) is shown in Figure S1 in the Supplemental Info.

The relative impacts of COVID-19 on off-road mobile source activities were also evaluated from port, railway, and aviation sectors. Port and rail activities were estimated as a relative reduction from prior year using container counts provided by the the port of Los Angeles, port of Long Beach, and freight rail companies. Time series of the change in container counts are provided in Figure S2 in the Supplemental Info. Aviation impacts were estimated as relative daily change from pre-pandemic baseline using Geotab data and counts provided by Los Angeles International Airport. A time series of the change in daily air carrier counts at Los Angeles International Airport is provided in Figure S3 in the Supplemental Info. Other off-road sectors such as agriculture, construction, and other off-road equipment were not evaluated in this study.

2.2 Estimating Changes in Mobile Source Emissions

EMFAC2017 (Emfac, 2017) was used as the foundational framework to provide a baseline on-road vehicle emission inventory in 2020 (i.e. estimated emissions for 2020 in the absence of COVID-19). Note that EMFAC2017 uses historical vehicle registration data until 2016, and vehicle activities in 2020 were forecasted. To calculate changes in emissions due to

COVID-19, Vehicle activity, or VMT scalers, relative changes to the baseline in January 2020, were generated based on VMT data as described in Section 2.1. In this study, it was assumed that the scalers of total VMT is representative of light-duty vehicle activity trends, as EMFAC2017 shows that 94% of the total VMT in California is from light-duty vehicles in 2020.

The VMT scalers were then applied to the EMFAC2017 baseline emission inventory in the SoCAB by vehicle class and by emission process. The changes in VMT were used as a surrogates to estimate changes in emissions from processes of running and idling exhaust, evaporative running loss, and brake wear and tire wear. Emissions for the rest of processes are not significantly influenced by vehicle distance traveled, and they are assumed to be the same as the case without COIVID-19 impact. It should be noted that emission rates vary by vehicle speed. With fewer vehicles on road, the average vehicle speed was observed to be higher during the study period. However, the impact of changes in vehicle speed was not included in this analysis due to lack of sufficient data.

2.3 Surface Monitoring Networks

In-situ measurements of O_3 and NO_2 from SoCAB monitoring sites shown in Figure 1 were accessed from CARB's Air Quality and Meteorological Information System (AQMIS2; https://www.arb.ca.gov/aqmis2/aqdselect.php). For O_3, data from 2000 through the end of the study period (July 2020) were accessed. Max Daily 8-hour O_3 (MDA8) values were calculated for each site for each day. The ratio of WE/WD O3 was calculated at each site using the ratio of period-average Max Daily 8-hour (MDA8) O_3 for Sundays versus Wednesdays. This methodology follows previous literature, which noted that Sundays tend to have the lowest VMT, while Wednsedays tend to have the highest (i.e. the difference between "Weekend" and "Weekday" emissions is maximized by using Sundays and Wednesdays as representative days) (Heuss et al., 2003; Yarwood et al., 2003; Wolff et al., 2013).

2.4 Satellite Data

To provide a broader spatial context for this study, column-integrated measurements of HCHO and NO_2 were obtained from the Ozone Monitoring Instrument (OMI) onboard NASA's Aura satellite. Daily L2 data products were obtained over California and filtered using the data quality flags and recommended QA/QC procedures (Readme, 2019; Lamsal et al., 2021; Readme, 2014). Both satellites provide daily observations at approximately 13:30 local time. For both OMI and TROPOMI, data were obtained from instrument launch through 2020 (i.e. 2005-2020 for OMI, 2018-2020 for TROPOMI). Both instruments provide pixels that vary in size depending on viewing geometry, but are a minimum of 13 x 24 km (OMI) and 3.5 x 5.5 km (TROPOMI) when viewed at nadir. For this work, we calculated the HCHO/NO_2 ratio for each observation (i.e. each pixel for each day) for each instrument. Additionally, much of this work utilizes daily spatial averages of satellite products, that is, the average value of all pixels contained within the SoCAB boundary on a given day. However, because NO_2 has a lognormal distribution, daily spatial averages of NO_2 and HCHO/NO_2 can be heavily skewed by the presence of cloudy or partly cloudy scenes. To account for this, data were smoothed by the following process: first, L2 data were temporally averaged to a fixed grid over a 15-day moving window centered on the measurement date (this provides a time-averaged map, 5 x 7 km for TROPOMI, and 13 x 24

for OMI). Then, the mean (for HCHO) or logarithmic mean (for NO_2 and $HCHO/NO_2$) of all moving-average grid cells that fell within the SoCAB boundary was calculated.

2.5 Model Configuration

Air quality model simulations over California from Feb 23 to July 5, 2020 were conducted using Community Multiscale Air
165 Quality (CMAQ) version 5.2.1 (Appel et al., 2013). The model runs for the first 7 days were considered as spin-up runs and excluded from the data analysis. SAPRC07TC and AERO6 mechanisms were used for gas and particle phase representations, respectively, in the CMAQ model. The modeling domain covers all of California and Nevada as well as part of the Pacific Ocean to the west. The modeling domain is comprised of 321 x 291 horizontal grids with a resolution of 4 x 4 km^2. The vertical grid is represented by 30 vertical layers from the land/ocean surface to 100mb. Default CMAQ initial conditions were used for
170 the model simulation. Chemical boundary conditions were derived from global chemical transport model Goddard Earth Observing System Model version 4 (MOZART-4) simulations conducted at the National Center for Atmospheric Research (NCAR)(Emmons et al., 2010). NCAR discontinued MOZART-4 simulations after January 2018 (https://www.acom.ucar.edu/wrf-chem/mozart.shtml), so 2017 data were mapped to the 2020 calendar, so the global impact of COVID-19 pandemic is not considered in these model simulations. Weather Research and Forecasting model (WRF) version
175 3.44.2.1 was used to provide meteorology fields as input for the CMAQ simulations (Skamarock et al., 2008). In the WRF model simulation, three nested domains with 36 x 36 km^2, 12 x 12 km^2 and 4 x 4 km^2 horizontal resolutions were employed. Outputs from the inner most 4 x 4 km^2 WRF domain were processed by MCIP version 4.3 to drive the CMAQ model.

To investigate the potential impacts of California's response to the COVID-19 pandemic on air quality in SoCAB, two sets of day specific 2020 emission inventories were prepared for this study. One represents the baseline emission inventory with
180 business as usual and no COVID-19 pandemic related adjustments. The second uses the 2020 baseline emissions as the starting point and then applies COVID-19 related adjustments to the on-road and off-road mobile emissions as described in Sections 2.1 and 2.2. Emission categories include on-road mobile, off-road mobile, area, elevated point, road dust and ocean going vessels. Biogenic emissions were prepared using the Model of Emissions and Gases and Aerosols from Nature v3.0 (MEGAN v3.0) (Guenther et al., 2006). Due a lack of leaf area index (LAI) data for 2020 at the time of study, 2018 LAI data with 2020
185 meteorology from WRF were used in MEGAN to estimate biogenic emissions.

In addition to the 2020 simulations, modeling of the 2010 CalNex study and previous regulatory related modeling activities at CARB are presented for 2010, 2012, 2015 and 2017 to study the long term trend of modeled WE/WD compared to observed WE/WD trends (Cai et al., 2019). The simulations for the four previous years utilized year-specific emission inventories and boundary conditions with CMAQv5.0.2. Other model configurations/settings were consistent with those for the 2020
190 simulations

3 Results

3.1 Changes in Precursor Emissions

3.1.1 Bottom-up: Impact of VMT on Emissions

Daily total emissions of NO_x and VOC in the SoCAB from baseline and COVID-19 adjusted emission inventories for the modeling period are shown in Figure 2~~Figure 2~~. For NO_x, the emissions with and without COVID-19 adjustment both show significant weekday vs. weekend variations with weekend emissions nearly 30-35% less than the weekday emissions. Compared to the baseline emissions, the decrease of NO_x emissions with COVID-19 adjustment started in early March, reached the maximum of -25% in early April, and slowly returned to around -5% by the end of June. The purple line in the top panel of Figure 2~~Figure 2~~ shows the reduction of NO_x emissions due to COVID-19 was generally higher on weekends than weekdays. Total VOC emissions were quite flat from March through the middle of April, when biogenic emissions generally contributed less than 50 tons per day towards total VOC emissions, or approximately 10-15% of the total VOC emissions. Starting from late April, there was a large increase in total VOC emissions which was due to the significant increase of biogenic emissions triggered by warmer temperatures. Biogenic emissions have large day-to-day variability, but averages ~230 tons per day over Summer, or aproximately one third of the total VOC emissions in the SoCAB. The percentage reduction of total VOC emissions due to COVID19 was much smaller compared to that for NO_x emissions. The maximum decrease of VOC emissions was around -6% in early April. There is no clear weekend vs. weekday variation for VOC emissions.

3.1.2 Top- down: Changes in ambient NO_2 after adjusting for meteorology

To validate the bottom-up emissions described in Section 3.1.1, we explored methods to provide a top-down estimate of the change in ambient NO_2 resulting from the COVID-19 response. The top-down estimate is complicated by the fact that changes in ambient NO_2 during 2020 are a combination of changes in meteorology, chemistry, and emissions. Historically, NO_2 concentrations in SoCAB decrease between February and June (See Figure 3); therefore, it is misleading to attribute the decline in NO_2 after the onset of pandemic to emissions changes alone. Furthermore, the timing of the seasonal decline in NO_2 varies from year to year, so comparison to the same month from previous years is problematic. For example, we compare the average NO_2 concentration between March 20th and June 20th in SoCAB (based on 21 sites with data through 2015 - 2020) for 2020 with the average NO_2 from each year between 2015 and 2019. This yields a wide range of -1.5 to -4.4 ppb for ΔNO_2 in 2020, relative to previous years. We improve on this estimate by using the Vehicle Miles Travelled (VMT) data as a predictor of activity change to provide a top-down estimate of the NO_2 changes attributable to emissions.

We construct a simple multivariate linear model to predict daily NO_2 concentrations based on relative humidity, wind speed, temperature, day of year, and day since January 1st, 2016 (to capture any long-term trends). The model is trained on hourly NO_2 data from 2016 – 2019 and used to predict daily NO_2 concentrations in 2020. The model predicts daily NO_2 in 2020 well ($r^2 = 0.82$, RMSE = 2.3 ppb); however, the model is typically biased high from March onwards. If we include VMT as a predictor variable (still only training on 2016 - 2019 data) the model more closely fits the observations in 2020 ($r^2 = 0.88$,

RMSE = 1.8 ppb). Figure 4Figure 4 (a) shows the time series of NO_2 from the observations and the model with and without VMT (left panel). In years prior to 2020, the model without VMT predicts the observed NO_2 to within 0.4 ppb and the addition
225 of VMT typically makes only a small difference (Figure 4Figure 4 (b)). In 2020, the model without VMT overestimates the NO_2 by 1.4 ppb relative to the observations. Including VMT provides a large correction to the model, underestimating by -0.4 ppb. We use the bounds to estimate that the ΔNO_2 resulting from emissions changes associated with the pandemic response are -1.4 to -1.8 ppb (or about 19% to 26%; the upper bound is the difference between the two models and assumes that the non-VMT model may overcompensate).

230 In parallel with the multivariate model, we use the historical relationship between detrended (7-day rolling average) VMT and NO_2 to infer the ΔNO_2 resulting from the ΔVMT (-17%) during the analysis period. The resulting ΔNO_2 via this method is -1.4 to -2.0 ppb, where the range is determined by the 95% confidence bounds of the Theil-Sen regression of detrended VMT and NO_2. The range is almost identical to the result from comparing the multivariate model with and without VMT, above. This contrasts with the estimate based on historical comparison alone (-1.5 to -4.4 ppb) that suggests a much larger upper
235 bound to the effect of the pandemic response on NO_2.

Finally, we compare the top-down estimate of the ΔNO_2 for 2020 with the ΔNO_2 from the 2020 CMAQ emissions inventory described in Section 3.1.1. The CMAQ ΔNO_2 is the difference between two simulations, both use the same meteorology but with 2017 versus 2020 emissions, averaged over the 21 South Coast sites used for the top-down comparison (and the same March 20th – June 20th time frame). The model produces a ΔNO_2 of -1.1 ppb when updated to 2020 emissions. This is slightly
240 below the top-down estimated range of -1.4 to -2.0 ppb. However, considering that 2020 meteorology was not used this suggests that the 2020 emissions used for the CMAQ modeling are reasonable.

3.2 In-Situ and Remote Sensing Observations

In Section 3.1, we quantified the changes in the O_3 precursor environment using a bottom-up and a top-down approach. These two approaches highlight that the abundance of NO_x was diminished in the April-July period of 2020, due to reductions in
245 mobile source emissions. This sections uses satellite data and surface monitoring networks to explore how this drastic change in precursor abundances affected regional O_3 chemistry.

3.2.1 Satellite HCHO/NO_2 as an Indicator of O_3 Sensitvity

Over polluted areas, both HCHO and NO_2 have vertical distributions that are heavily weighted toward the lower troposphere, meaning that column-integrated satellite measurements of these gases are fairly representative of near-surface conditions.
250 Many studies have taken advantage of these favorable vertical distributions to invesitigate surface emissions of NO_x and VOCs from space (Duncan et al., 2016; Krotkov et al., 2015; Duncan et al., 2010; Martin et al., 2004; Fishman et al., 2008). Recent literature has shown that the HCHO/NO_2 ratio can be a useful indicator of regional O_3 sensitivity, although the uncertainty associated with the technique is sufficiently high such that use of the ratio should be reserved for qualitative evaluation of spatiotemporal trends (Schroeder et al., 2017; Jin et al., 2020). In general, very low ratios are associated with VOC-limited

conditions, and very high ratios are associated with NO_x-limited conditions. In Figure 5 (left panel), we show that the OMI HCHO/NO_2 ratio in the SoCAB generally increased from 2005 – 2020. Given that previous studies had identified the SoCAB as VOC-limited during the mid 2000's, we can conclude that the increasing HCHO/NO_2 ratio in Figure 5 indicates that the SoCAB has been becoming less VOC-limited over time, which is consistent with recent literature (Pollack et al., 2012). However, this information alone is not enough to conclude whether the region had shifted to a NO_x-limited environment by the end of the time series. Figure 5 (right panel) shows the de-trended seasonality of the OMI HCHO/NO_2 ratio from 2005 – 2020. In general, lower HCHO/NO_2 ratios occurred during Spring compared to Summer, with the increase and plateau corresponding to the seasonality of biogenic emissions in the region (Dreyfus et al., 2002; Misztal et al., 2014). This suggests that, for a given year, Spring (April – May) would appear more VOC-limited than Summer (June – July), and vice-versa.

While Figure 5 demonstrates the qualitative utility of the HCHO/NO_2 ratio for exploring interannual and seasonal trends, classification into NO_x-limited or VOC-limited regimes can be achieved by coupling this ratio with O_3 data from surface monitoring networks. Figure 6 utilizes daily HCHO/NO_2 ratios (spatially aggregated over the SoCAB) coupled with daily MDA8 O_3 data from the surface monitoring network. These data are binned into five-year increments and separated by season. When presented this way, increasing and decreasing trends within a bin can be used to identify VOC-limited versus NO_x-limited regimes, respectively. In a region that is firmly VOC-limited, HCHO/NO_2 ratios are expected to have a positive relationship with MDA8 O_3 – that is, days with higher O_3 are expected to occur on days with higher HCHO/NO_2 ratios (i.e., closest to the "transitional" regime where O_3 production is maximized along a ridgeline). In a NO_x-limited environment, the opposite would be expected, where high O_3 days are expected to occur on days with lower HCHO/NO_2 ratios (in a NO_x-limited environment, lower HCHO/NO_2 ratios would be closer to the "transitional" state where O_3 production is maximized along a ridgeline). Using these expected tendencies as indicators, we can identify seasons and years that were VOC-limited, such as Spring 2005 – 2009, Summer 2005 – 2009, and Spring 2010 – 2014. Spring of 2015 – 2019 and Summer of 2010 – 2014 had no apparent trends (likely indicative of "transitional" states), while Summer 2015 – 2019 showed a slight negative trend, which could be indicative of a weakly NO_x-limited photochemical regime. In contrast, both Spring and Summer of 2020 showed strong negative trends, with high O_3 days associated with lower HCHO/NO_2 ratios. Taken together, this implies that Spring of 2020 was likely the first Spring season to be NO_x-limited since records began, while Summer likely moved from a weakly NO_x-limited regime in 2015 - 2019 years to a firmly NO_x-limited regime in 2020.

3.2.2 The O_3 Weekend/Weekday Effect

While the satellite-based approach presented in Section 3.2.1 is useful for diagnosing O_3 sensitivity at regional scales, there are subtle nuances that cannot be accounted for using the satellite-based approach alone. First, satellite instruments, particularly OMI, have relatively coarse spatial resolution and have limited utility for diagnosing sub-regional gradients in O_3 sensitivity. While exploring O_3 chemistry aggregated to the regional scale is certainly useful, additional information about the location of sub-regional gradients in O_3 sensitivity can be useful for understanding policy implications when coupled with knowledge of emission sources, population centers, and typical meteorology. Secondly, polar orbiting satellites overpass once per day,

typically around midday (OMI's orbit passes over California around 13:30 local time), making it impossible to diagnose diurnal trends in O_3 sensitivity from satellite data alone. Ambient O_3 concentrations typically peak in the late afternoon and are the

290 result of chemical production integrated over the course of the day, with midday chemistry appearing more NO_x-limited in character than other times of day (due to higher actinic flux, higher temperatures, higher biogenic emissions, and reduced NO_x emissions relative to morning and evening commute times). Applying WE/WD analysis to surface monitoring networks (described in Section 2) enables exploration of sub-regional gradients in O_3 chemistry. Furthermore, because this approach only employs MDA8 O_3, WE/WD analysis inherently contains information about the outcomes of diurnally-integrated

295 photochemistry. Figure 7 shows the long-term trend in the WE/WD effect in Springtime (left panel) and Summertime (right panel). O_3 monitor data is available prior to 2005, but the time period and binning method shown in Figure 7 were chosen to be consistent with Figure 6. In Figure 7, blue colors (i.e. weekend O_3 higher than weekday O_3) are indicative of locally VOC-limited conditions, whereby reductions in NO_x on weekends coincided with higher ambient O_3. Orange colors are an indication of locally NO_x-limited conditions, whereby reductions in NO_x on weekends coincided with lower ambient O_3.

300 In general, the trends shown in Figure 7 agree with those presented in Section 3.2.1. Spring of 2005 – 2019 appear VOC-limited, though the effect was weakening with lighter shades of blue present in Spring 2015 – 2019. The analysis in Section 3.2.1 labeled Spring 2015 – 2019 as "transitional", while analysis of Figure 7 concludes that this period was likely weakly VOC-limited. Summer of 2005 – 2014 was generally VOC-limited with most monitors having WE/WD ratios below 1. However, by Summer of 2015 – 2019, many monitoring sites had WE/WD ratios above 1, indicative of NO_x-limited conditions.

305 The spatially-aggregated approach employed in Section 3.2.1 concluded that Summer 2015 – 2019 was weakly NO_x-limited at the regional scale, however, using the WE/WD ratios in Figure 7, interesting sub-regional gradients are noted. For example, while most sites in Summer 2015 – 2019 had WE/WD ratios below 1, a concentration of monitoring sites near the urban core of LA and the LA/Long Beach corridor had WE/WD ratios above 1. This region is a strong source of NO_x emissions from mobile sources, including HDV traffic from the port of Los Angeles and port of Long Beach. This highlights the difficulty in

310 controlling O_3 in VOC-limited environments: urban core areas may lag the broader region in transitioning from VOC-limited to NO_x-limited, which may have important outcomes with respect to the spatial distribution of O_3 and O_3 exposure.

In Spring of 2020, every monitor in the SoCAB was characterized as having WE/WD ratios below 1. Surprisingly, this includes the urban core of LA and the LA/Long Beach truck corridor. While O_3 chemistry in Springtime is generally more VOC-limited in nature than in Summertime (i.e. right panel of Figure 5), the deepest reductions in NO_x emissions due to COVID-19 were

315 observed in Springtime (up to 25% reduction, i.e. Figure 3), implying that COVID-19-related mobile source reductions were of a large enough magnitude to alter the Springtime photochemical environment. This agrees with the satellite-based analysis presented in Figure 6. In Summertime of 2020, all but two of the monitoring sites had WE/WD ratios below 1. This includes the urban core of LA and the LA/Long Beach corridor, which had WE/WD ratios above 1 in every year prior to 2020. While Summertime NO_x emissions were not reduced by as much as Springtime NO_x emissions in 2020 (i.e. Figure 2Figure 2), the

320 baseline Summertime photochemistry was already weakly NO_x-limited (i.e. Summer 2015-2019). This implies that the mobile

source reductions attributed to COVID-19 were sufficient to change Summertime photochemistry from "weakly NO_x-limited" to "firmly NO_x-limited", including the urban core of LA and the LA/Long Beach corridor.

3.3 Modelling Results

While analysis of satellite and surface monitor data reveal that COVID-related NO_x reductions were sufficient to push the SoCAB into a NO_x-limited regime in both Spring and Summer of 2020, understanding the implications of this photochemical shift on ambient O_3 levels requires further consideration. For example, present-day satellites are only capable of measuring HCHO and NO_2 once per day, typically around midday. While these satellite data are nonetheless useful, one must consider that MDA8 O_3 is the result of diurnally-integrated O_3 production, meaning that the current generation of satellites do not provide a complete picture. Additionally, meteorology makes interpretation of indicators difficult. It is well-documented that downwind areas in the Eastern part of the SoCAB typically experience the highest MDA8 O_3 in the basin; therefore, it can be difficult to connect observed WE/WD ratios at receptor sites to photochemical conditions at source regions. Recent papers have analyzed spatiotemporal trends of NO_2 in the SoCAB during the COVID period, and all noted that short-term meteorological variability makes it challenging to draw comparisons against recent years (Naeger and Murphy, 2020; Parker et al., 2020; Goldberg et al., 2020). Parker et al. (2020) concluded that NO_x reductions during the COVID period were not associated with meaningful changes in SoCAB O_3 concentrations, however, short-term meteorological variability can also obscure the effects that short-term changes in O_3 sensitivity impart on ambient O_3 levels. We expand upon these papers by using a compilation of chemical transport model simulations to disentangle the effects of emissions, chemistry, and meteorology on ambient O_3 levels during the study period. A statistical evaluation of the model's skill in simulating meteorological conditions across the SoCAB during the study period is provided in the Supplemental Info. In Sections 3.3.1 and 3.3.2, we highlight that these model simulations were able to accurately capture the long-term change in O_3 sensitivity over the past decade, and accurately simulated the O_3 precursor environment in 2020. With this information in hand, we use two sets of simulations (base-case and COVID-adjusted emissions) to isolate and quantify the change in O_3 that can be attributed to COVID precautions.

3.3.1 Multiyear Simulations of the WE/WD Effect on O_3

CMAQ has been used to simulate California O_3 concentrations for 2010, 2012, 2015, 2017 and 2020 (Cai et al., 2019). The calculated WE/WD ratios of MDA8 O_3 from model simulations for these years are compared with the observed ratios at the monitoring sites in SoCAB for April to July. Calculation of WE/WD ratios follows the procedure described in Section 2. The boxplots in Figure 8Figure 8 show the variation of observed April-July O_3 WE/WD ratios among SoCAB monitoring sites from 2000 to 2020. The solid black lines in the box are the mean WE/WD ratios of all the sites for each year. The red dots in Figure 8Figure 8 are modeled mean O_3 WE/WD ratios for the corresponding years. The 2020 modeled data is from the simulation with COVID-19 adjusted emissions. With year-by-year variations, the long term trend of O_3 WE/WD ratios shows a general decrease during the past two decades. Compared to the majority of the earlier years, the observed mean ratios after

2014 are much closer to 1.0 with the mean ratios for 2016, 2018 and 2020 all below 1. Model simulated mean O_3 WE/WD ratios are very consistent with the observed mean ratios indicating the modeling system captured the change of chemical regime over the years. The difference between modeled and observed mean ratios for 2020 is larger than the difference for the other years, with the model predicting a higher WE/WD ratio than observed. This may indicate that, while the model captured the transition to a NO_x-limited photochemical environment, modeled MDA8 O_3 may be slightly less sensitive to changes in NO_x than is observed. Detailed model performance comparing simulated to observed NO_2 in 2020 is shown in the following section.

3.3.2 Model Simulations for NO_2 and O_3 during the COVID-19 period

For the COVID-19 period in 2020, we analysed times series of NO_2 and O_3 from model simulations as well as a comparison with observations from ground monitoring sites. The difference between the two model simulations with and without COVID-19 adjustment reflects the impact of COVID-19 emission reductions. The left top panel of Figure 9Figure 9 shows the daily average NO_2 concentrations from observations and the model simulations with COVID-19 adjusted emissions. The right top panel of Figure 9Figure 9 shows the NO_2 difference between the two model simulations (COVID-19 adjusted – baseline). Since observed NO_2 at a monitoring site can be heavily impacted by the local emissions but modeled data are diluted concentrations in 4 x 4 km^2 grids, for the NO_2 model comparison with observation we considered 18 non-near road monitoring sites. As shown in Figure 9Figure 9, the model captures the day-to-day variations of NO_2 reasonably well. The normalized mean biases of NO_2 for March, April, May and June are -24%, -8%, -4% and 1% respectively. The larger model bias in March is due to the significant model under estimations during the second and third weeks of March when there was rain. The difference between simulated NO_2 using COVID-19 adjusted emission inventory and baseline emission shows that NO_2 concentration was reduced by up to 2.6 ppb due to the COVID-19 emission reduction where the maximum reduction occurred on March 31. During April and early May, the NO_2 reduction was generally between 1 to 2 ppb. After May 10, the reduction of NO_2 continued to be smaller and becomes nearly diminished by the end of June.

Observed and model simulated MDA8 O_3 concentrations are shown in the left (bottom) of Figure 9Figure 9. Larger discrepancies between model and observation can be seen for the second and third weeks of March as well as the second week of April when O_3 concentrations are generally low. Those two time periods were associated with two rain events, above average cloud coverage and relative humidity as well as below average temperature. From mid-April to the end of June when O_3 concentrations were relatively higher, modeled O_3 concentrations are in very nice agreement with the observations. Significant enhancement of O_3 was observed during late April and early May. This O_3 enhancement was successfully captured by the model except that the peak O_3 concentrations on May 6 and 7 were under predicted in the model consistent with the under prediction of NO_2 during these days. During the late April to early May, high pressure ridges were the dominant weather patterns over SoCAB. The region had weak offshore winds, low planetary boundary layer height and extremely high temperatures, which favor the production and accumulation of O_3. The highest average daily maximum temperature from all the monitoring sites reached 33.5 °C on May 6 in both the observations and model simulation. The O_3 difference between model simulations with COVID-19 adjusted emissions and baseline emissions is illustrated in the right bottom panel of Figure

9Figure 9. The COVID-19 emission reduction caused the O_3 concentration to increase by up to 1.2 ppb from March to mid-April and mostly decrease by up to 2 ppb from late April to early July. On May 7 when the highest O_3 was observed, the O_3 concentrations were reduced by about 1.7 ppb due to the COVID-19 emission reductions. The change in O_3 difference between the two model simulations over time, especially the shift from positive to negative, indicates the transition from VOC-limited chemical regime to more NO_x-limited chemical regime.

4 Discussion

Using a multi-perspective approach involving satellites, surface monitors, and modeling, we show that the SoCAB was on average NO_x-limited during the COVID-19 period in April – July of 2020. While satellite data and the weekend/weekday effect suggest that Summertime in recent years may have been slightly NO_x-limited even before COVID-related mobile source reductions, Spring of 2020 was the first Spring on record to display NO_x-limited characteristics. This outcome was achieved by relatively large emissions reductions in Springtime (~20% reduction in SoCAB NO_x emissions), which was sufficient to offset the typical climatology of O_3 sensitivity in the region. In Summertime, when O_3 sensitivity is naturally more NO_x-limited than in Spring (a combination of biogenic emissions, warmer temperatures, and higher actinic flux), a 5% reduction in SoCAB NO_x emissions due to COVID-19 acted to push the region further into NO_x-limted territory. In both Spring and Summer of 2020, reductions in mobile source emissions due to COVID-related precautions were the largest contributor to regional NO_x emissions reductions. Thus, the natural experiment offered by data collected during the COVID-19 period of 2020 highlights that reductions in mobile source emissions alone could be a feasible pathway for shifting the SoCAB into a NO_x-limited O_3 production regime.

This work builds on recent studies that focused on the impacts of COVID-related precautions on O_3 and its precursors in Southern California. Naeger et al. (2020) compared TROPOMI NO_2 levels in Spring of 2020 to levels observed in Spring of 2019. While the authors excluded wet periods from their analysis, the 40% reduction that they report in Los Angeles is higher than similar studies that attempted to better-account for meteorology, such as Goldberg et al. (2020), who reported a 32% reduction in TROPOMI NO_2 for Los Angeles. In Section 3, our bottom-up approach using measurements of vehicle activity yielded an estimated NO_x emissions reduction of 25% during the deepest point of the shutdown, with typical reductions of ~15-20% during Springtime and ~5% during Summertime. While our bottom-up estimate of the reduction in NO_x emissions due to COVID-19 is lower than those reported in Naeger et al. (2020) and Goldberg et al (2020), there are important considerations that must be made to address this discrepancy. First, both Naeger et al. (2020) and Goldberg et al. (2020) focused on city-scale observations, which included the city of Los Angeles rather than the broader SoCAB region focused on in this study. Naeger et al. (2020) showed that NO_2 reductions were strongest in the urban core, therefore the numbers reported in Naeger (2020) and Goldberg (2020) would likely decrease if expanded to the broader SoCAB region. Secondly, ambient NO_2 levels are a function of both emissions and removal. As shown in this work, reduced NO_x emissions produced a fundamental shift in the underlying photochemistry of the region, which could lead to a decrease in the NO_x lifetime due to

enhanced photochemical cycling. Therefore, a given decrease in the NO_x emission rate could be concurrent with an increase in the NO_x removal rate, leading to a larger observed decrease in ambient NO_2 than can be explained by emissions alone.

420   Recent work by Parker et al. (2020) and Parker et al. (2022) also analyzed O_3 and its precursors in the SoCAB during the COVID-19 'stay at home order.' by integrating satellite measurements and surface measurements. Both papersThe authors concluded that the NO_x reductions observed during that period in the SoCAB were not sufficient to reduce O_3 levels across the basin, and Parker et al. (2020) instead advocate for VOC controls concurrent with NO_x reductions as a pathway for controlling O_3. Parker et al. (2022) noted an O_3 increase in the urban core of the SoCAB which is seemingly in contrast to our

425   work, however, when their results are averaged over the whole SoCAB (as in our work), a minor decrease in O_3 is observed. This result highlights the importance of spatial scales when considering O_3 chemistry: While we find that O_3 chemistry at the basin-scale indeed shifted to a NO_x-limited regime and produced modest decreases in ambient O_3, this should not be taken to mean that these observations were uniform across the basin. The combination of our work with the work of Parker et al. (2022) suggests that future reductions in NO_x emissions will be, on average, beneficial towards reducing ambient O_3 in the SoCAB.

430   However, this benefit may not play out evenly across the basin, and certain sub-regions will likely lag behind others in seeing improvements.

    However, It should be noted that both Parker et al. (2020) and Parker et al. (2022) drew their conclusions about O_3 chemistry by focusinged on the outcome (i.e., ambient O_3 concentrations) and used that to infer about the underlying process (i.e., O_3 chemical regime). The work presented here focuses on identifying the underlying chemical regime using process-based

435   indicators rather than outcome-based indicators. It should be noted that, at the chemical process level, there are many scenarios where O_3 chemistry may "flip" from VOC-limited to NOx-limited while still producing an increase in O_3 due to non-linearities in chemistry alone, especially when dealing with airmasses that are near the chemical transition point. Therefore, Parker's observation that O_3 increased in some areas while NO_x emissions dropped is not a solid indicator of the underlying chemical regime (especially given that the SoCAB is near the chemical transition point). Our work expands upon the work in Parker at

440   el. (2020Parker's work) by including the satellite HCHO/NO_2 ratio as an process-based indicator of regional O_3 sensitivity and by performing model simulations with base-case versus COVID-adjusted emissions. While our conclusions generally agree with Parker et al. (2020) and Parker et al. (2022), our finding that on average the SoCAB transitioned into a NO_x-limited regime in both Spring and Summer of 2020 cannot be understated. While reaching NO_x-limited territory is certainly not the same as reaching regional O_3 attainment, it is nonetheless an important milestone from a regulatory perspective. The fact that

445   O_3 levels in April – July of 2020 were not particularly different from recent years does indeed suggest that NO_x reductions similar to those observed in 2020 would not be sufficient for meaningful O_3 improvements to be realized. However, our modeling experiment suggests that COVID-related NO_x reductions resulted in O_3 levels that were 0-2 ppb lower than they would have been in April – July in the absence of COVID-related precautions. The fact that the SoCAB shifted to a NO_x-limited regime and experienced a reduction in simulated O_3 (per our modeling study) emphasizes that drastic reductions in

450   NO_x emissions (more than the reductions observed in 2020) will be effective in reducing ambient O_3 (though response on any given day or site may differ from the basin and/or seasonal average conditions). This finding is well-aligned with recent state

legislation, such as the Heavy-Duty Omnibus Regulation (https://ww2.arb.ca.gov/rulemaking/2020/hdomnibuslowNOx) and the Governor's Exeutive Order mandating that all new light-duty vehicle sales be zero emission by 2035, with heavy-duty sales to follow by 2045 (https://www.gov.ca.gov/wp-content/uploads/2020/09/9.23.20-EO-N-79-20-Climate.pdf). While
455 Parker et al. (2020) is correct that concurrent reductions in VOC emissions will also be beneficial for controlling O_3, a large portion of SoCAB VOC emissions during O_3 season are biogenic in nature (approximately one third or more by mass), implying that significant reductions in ambient O_3 can only be achieved with drastic reductions in NO_x emissions.

Achieving attainment for O_3 air quality standards will be further complicated by the enhanced frequency of drought and heat waves that California is expected to experience due to a changing climate (Swain et al., 2014). While short-term heat waves
460 result in enhanced photochemical activity and are typically associated with the highest O_3 values of a season (for example, the heat wave highlighted in Section 3.3.2), multi-year droughts are believed to inhibit biogenic VOC emissions, which could lead to reductions in O_3 production (Demetillo et al., 2019). While this study shows that statewide efforts to drastically reduce mobile source NO_x emissions will be effective for long-term reductions in ambient O_3 in the SoCAB, the effectiveness of such policies may be partially obscured by short-term meteorological variability and long-term climate change. Disentangling these
465 climatic effects from the effects of regulations will be a challenge for scientists and policymakers in the next decades. Follow-up studies will likely require novel fusions of observation systems including climate models, ultra-high-resolution chemical transport models, geostationary satellites, and dense monitoring networks.

References

Appel, K. W., Pouliot, G. A., Simon, H., Sarwar, G., Pye, H. O. T., Napelenok, S. L., Akhtar, F., and Roselle, S. J.: Evaluation
470 of dust and trace metal estimates from the Community Multiscale Air Quality (CMAQ) model version 5.0, Geosci. Model Dev., 6, 883-899, 10.5194/gmd-6-883-2013, 2013.

South Coast AQMD: Final 2016 Air Quality Management Plan: https://www.aqmd.gov/docs/default-source/clean-air-plans/air-quality-management-plans/2016-air-quality-management-plan/final-2016-aqmp/final2016aqmp.pdf?sfvrsn=15, last access: March, 2021.

475 Barletta, B., Meinardi, S., Kenseth, C. M., Schulze, B., Parker, H., Crounse, J. D., Wennberg, P. O., Barsanti, K., Seinfeld, J., and Blake, D. R.: VOC levels in the Los Angeles basin: impact of COVID-19 restrictions, AGU Fall Meeting 2020,

Cai, C., Avise, J., Kaduwela, A., DaMassa, J., Warneke, C., Gilman, J. B., Kuster, W., de Gouw, J., Volkamer, R., and Stevens, P.: Simulating the weekly cycle of NOx-VOC-HOx-O3 photochemical system in the South Coast of California during CalNex-2010 campaign, Journal of Geophysical Research: Atmospheres, 124, 3532-3555, 2019.

480 CalTrans Data WIM: https://dot.ca.gov/programs/traffic-operations/wim/data-wim, last access: February.

CalTrans Performance Measurement System (PeMS) Data Source: https://dot.ca.gov/programs/traffic-operations/mpr/pems-source, last access: February.

Chameides, W. and Walker, J. C. G.: A photochemical theory of tropospheric ozone, Journal of Geophysical Research (1896-1977), 78, 8751-8760, https://doi.org/10.1029/JC078i036p08751, 1973.

485   Chameides, W. L., Fehsenfeld, F., Rodgers, M. O., Cardelino, C., Martinez, J., Parrish, D., Lonneman, W., Lawson, D. R., Rasmussen, R. A., Zimmerman, P., Greenberg, J., Mlddleton, P., and Wang, T.: Ozone precursor relationships in the ambient atmosphere, Journal of Geophysical Research: Atmospheres, 97, 6037-6055, https://doi.org/10.1029/91JD03014, 1992.

Demetillo, M. A. G., Anderson, J. F., Geddes, J. A., Yang, X., Najacht, E. Y., Herrera, S. A., Kabasares, K. M., Kotsakis, A. E., Lerdau, M. T., and Pusede, S. E.: Observing Severe Drought Influences on Ozone Air Pollution in California,
490   Environmental Science & Technology, 53, 4695-4706, 10.1021/acs.est.8b04852, 2019.

Dreyfus, G. B., Schade, G. W., and Goldstein, A. H.: Observational constraints on the contribution of isoprene oxidation to ozone production on the western slope of the Sierra Nevada, California, Journal of Geophysical Research: Atmospheres, 107, ACH 1-1-ACH 1-17, https://doi.org/10.1029/2001JD001490, 2002.

Duncan, B. N., Lamsal, L. N., Thompson, A. M., Yoshida, Y., Lu, Z., Streets, D. G., Hurwitz, M. M., and Pickering, K. E.: A
495   space-based, high-resolution view of notable changes in urban NOx pollution around the world (2005–2014), Journal of Geophysical Research: Atmospheres, 121, 976-996, https://doi.org/10.1002/2015JD024121, 2016.

Duncan, B. N., Yoshida, Y., Olson, J. R., Sillman, S., Martin, R. V., Lamsal, L., Hu, Y., Pickering, K. E., Retscher, C., Allen, D. J., and Crawford, J. H.: Application of OMI observations to a space-based indicator of NOx and VOC controls on surface ozone formation, Atmospheric Environment, 44, 2213-2223, https://doi.org/10.1016/j.atmosenv.2010.03.010, 2010.

500   EMFAC 2017 - Emissions Inventory: https://arb.ca.gov/emfac/emissions-inventory, last access: 3/17/2021.

Emmons, L. K., Walters, S., Hess, P. G., Lamarque, J. F., Pfister, G. G., Fillmore, D., Granier, C., Guenther, A., Kinnison, D., Laepple, T., Orlando, J., Tie, X., Tyndall, G., Wiedinmyer, C., Baughcum, S. L., and Kloster, S.: Description and evaluation of the Model for Ozone and Related chemical Tracers, version 4 (MOZART-4), Geosci. Model Dev., 3, 43-67, 10.5194/gmd-3-43-2010, 2010.

505   Fishman, J., Bowman, K. W., Burrows, J. P., Richter, A., Chance, K. V., Edwards, D. P., Martin, R. V., Morris, G. A., Pierce, R. B., Ziemke, J. R., Al-Saadi, J. A., Creilson, J. K., Schaack, T. K., and Thompson, A. M.: Remote Sensing of Tropospheric Pollution from Space, Bulletin of the American Meteorological Society, 89, 805-822, 10.1175/2008bams2526.1, 2008.

Fujita, E. M., Campbell, D. E., Stockwell, W. R., and Lawson, D. R.: Past and future ozone trends in California's South Coast Air Basin: reconciliation of ambient measurements with past and projected emission inventories, J Air Waste Manag Assoc,
510   63, 54-69, 10.1080/10962247.2012.735211, 2013.

Fujita, E. M., Campbell, D. E., Stockwell, W. R., Saunders, E., Fitzgerald, R., and Perea, R.: Projected ozone trends and changes in the ozone-precursor relationship in the South Coast Air Basin in response to varying reductions of precursor emissions, J Air Waste Manag Assoc, 66, 201-214, 10.1080/10962247.2015.1106991, 2016.

Goldberg, D. L., Anenberg, S. C., Griffin, D., McLinden, C. A., Lu, Z., and Streets, D. G.: Disentangling the Impact of the
515   COVID-19 Lockdowns on Urban NO2 From Natural Variability, Geophysical Research Letters, 47, e2020GL089269, https://doi.org/10.1029/2020GL089269, 2020.

Guenther, A., Karl, T., Harley, P., Wiedinmyer, C., Palmer, P. I., and Geron, C.: Estimates of global terrestrial isoprene emissions using MEGAN (Model of Emissions of Gases and Aerosols from Nature), Atmospheric Chemistry and Physics, 6, 3181-3210, 2006.

520   Heuss, J. M., Kahlbaum, D. F., and Wolff, G. T.: Weekday/weekend ozone differences: what can we learn from them?, Journal of the Air & Waste Management Association, 53, 772-788, 2003.

Jin, X., Fiore, A., Boersma, K. F., Smedt, I., and Valin, L.: Inferring Changes in Summertime Surface Ozone-NOx-VOC Chemistry over U.S. Urban Areas from Two Decades of Satellite and Ground-Based Observations, Environ Sci Technol, 54, 6518-6529, 10.1021/acs.est.9b07785, 2020.

525 Kleinman, L. I., Daum, P. H., Lee, J. H., Lee, Y.-N., Nunnermacker, L. J., Springston, S. R., Newman, L., Weinstein-Lloyd, J., and Sillman, S.: Dependence of ozone production on NO and hydrocarbons in the troposphere, Geophysical Research Letters, 24, 2299-2302, https://doi.org/10.1029/97GL02279, 1997.

Krotkov, N., McLinden, C., Li, C., Lamsal, L., Celarier, E., Marchenko, S., Swartz, W., Bucsela, E., Joiner, J., and Duncan, B.: Aura OMI observations of regional SO 2 and NO 2 pollution changes from 2005 to 2014, Atmospheric Chemistry & 530 Physics Discussions, 15, 2015.

Lamsal, L. N., Krotkov, N. A., Vasilkov, A., Marchenko, S., Qin, W., Yang, E. S., Fasnacht, Z., Joiner, J., Choi, S., Haffner, D., Swartz, W. H., Fisher, B., and Bucsela, E.: Ozone Monitoring Instrument (OMI) Aura nitrogen dioxide standard product version 4.0 with improved surface and cloud treatments, Atmos. Meas. Tech., 14, 455-479, 10.5194/amt-14-455-2021, 2021.

Martin, R. V., Fiore, A. M., and Van Donkelaar, A.: Space-based diagnosis of surface ozone sensitivity to anthropogenic 535 emissions, Geophysical Research Letters, 31, https://doi.org/10.1029/2004GL019416, 2004.

Misztal, P. K., Karl, T., Weber, R., Jonsson, H. H., Guenther, A. B., and Goldstein, A. H.: Airborne flux measurements of biogenic isoprene over California, Atmos. Chem. Phys., 14, 10631-10647, 10.5194/acp-14-10631-2014, 2014.

Naeger, A. R. and Murphy, K.: Impact of COVID-19 Containment Measures on Air Pollution in California, Aerosol and Air Quality Research, 20, 2025-2034, 10.4209/aaqr.2020.05.0227, 2020.

540 Parker, H. A., Hasheminassab, S., Crounse, J. D., Roehl, C. M., and Wennberg, P. O.: Impacts of Traffic Reductions Associated With COVID-19 on Southern California Air Quality, Geophys Res Lett, 47, e2020GL090164, 10.1029/2020gl090164, 2020.

Parker, L. K., Johnson, J., Grant, J., Vennam, P., Chien, C-J., and Morris, R.: Ozone Trends and the Ability of Models to Reproduce the 2020 Ozone Concentrations in the South Coast Air Basin in Southern California under the COVID-19 Restrictions, Atmosphere, 13, 10.3390/atmos13040528, 2022.

545 Pollack, I. B., Ryerson, T. B., Trainer, M., Neuman, J. A., Roberts, J. M., and Parrish, D. D.: Trends in ozone, its precursors, and related secondary oxidation products in Los Angeles, California: A synthesis of measurements from 1960 to 2010, Journal of Geophysical Research: Atmospheres, 118, 5893-5911, https://doi.org/10.1002/jgrd.50472, 2013.

Pollack, I. B., Ryerson, T. B., Trainer, M., Parrish, D. D., Andrews, A. E., Atlas, E. L., Blake, D. R., Brown, S. S., Commane, R., Daube, B. C., de Gouw, J. A., Dubé, W. P., Flynn, J., Frost, G. J., Gilman, J. B., Grossberg, N., Holloway, J. S., Kofler, J., 550 Kort, E. A., Kuster, W. C., Lang, P. M., Lefer, B., Lueb, R. A., Neuman, J. A., Nowak, J. B., Novelli, P. C., Peischl, J., Perring, A. E., Roberts, J. M., Santoni, G., Schwarz, J. P., Spackman, J. R., Wagner, N. L., Warneke, C., Washenfelder, R. A., Wofsy, S. C., and Xiang, B.: Airborne and ground-based observations of a weekend effect in ozone, precursors, and oxidation products in the California South Coast Air Basin, Journal of Geophysical Research: Atmospheres, 117, https://doi.org/10.1029/2011JD016772, 2012.

555 OMHCHO README FILE: https://aura.gesdisc.eosdis.nasa.gov/data/Aura_OMI_Level2/OMHCHO.003/doc/README.OMHCHO.pdf, last access: March.

OMNO2 README Document Data Product Version 4.0: https://aura.gesdisc.eosdis.nasa.gov/data/Aura_OMI_Level2/OMNO2.003/doc/README.OMNO2.pdf, last access: March.

560 Schroeder, J. R., Crawford, J. H., Fried, A., Walega, J., Weinheimer, A., Wisthaler, A., Müller, M., Mikoviny, T., Chen, G., Shook, M., Blake, D. R., and Tonnesen, G. S.: New insights into the column CH2O/NO2 ratio as an indicator of near-surface ozone sensitivity, Journal of Geophysical Research: Atmospheres, 122, 8885-8907, https://doi.org/10.1002/2017JD026781, 2017.

Sillman, S., Logan, J. A., and Wofsy, S. C.: The sensitivity of ozone to nitrogen oxides and hydrocarbons in regional ozone 565 episodes, Journal of Geophysical Research: Atmospheres, 95, 1837-1851, https://doi.org/10.1029/JD095iD02p01837, 1990.

Skamarock, W. C., Klemp, J. B., Dudhia, J., Gill, D. O., and Barker, D.: A Description of the Advanced Research WRF Version 3 University Corporation for Atmospheric ResearchNo. NCAR/TN-475+STR, doi:10.5065/D68S4MVH, 2008.

Streetlight: Our Methodology and Data Sources: https://learn.streetlightdata.com/methodology-data-sources-white-paper, last access: February.

570 Swain, D. L., Tsiang, M., Haugen, M., Singh, D., Charland, A., Rajaratnam, B., and Diffenbaugh, N. S.: The extraordinary California drought of 2013/2014: Character, context, and the role of climate change, Bull. Am. Meteorol. Soc, 95, S3-S7, 2014.

CEPAM: 2016 SIP - Standard Emission Tool: https://www.arb.ca.gov/app/emsinv/fcemssumcat/fcemssumcat2016.php, last access: 3/17/2021.

575 Wolff, G. T., Kahlbaum, D. F., and Heuss, J. M.: The vanishing ozone weekday/weekend effect, Journal of the Air & Waste Management Association, 63, 292-299, 10.1080/10962247.2012.749312, 2013.

Yarwood, G., Stoeckenius, T. E., Heiken, J. G., and Dunker, A. M.: Modeling weekday/weekend ozone differences in the Los Angeles region for 1997, Journal of the Air & Waste Management Association, 53, 864-875, 2003.

580
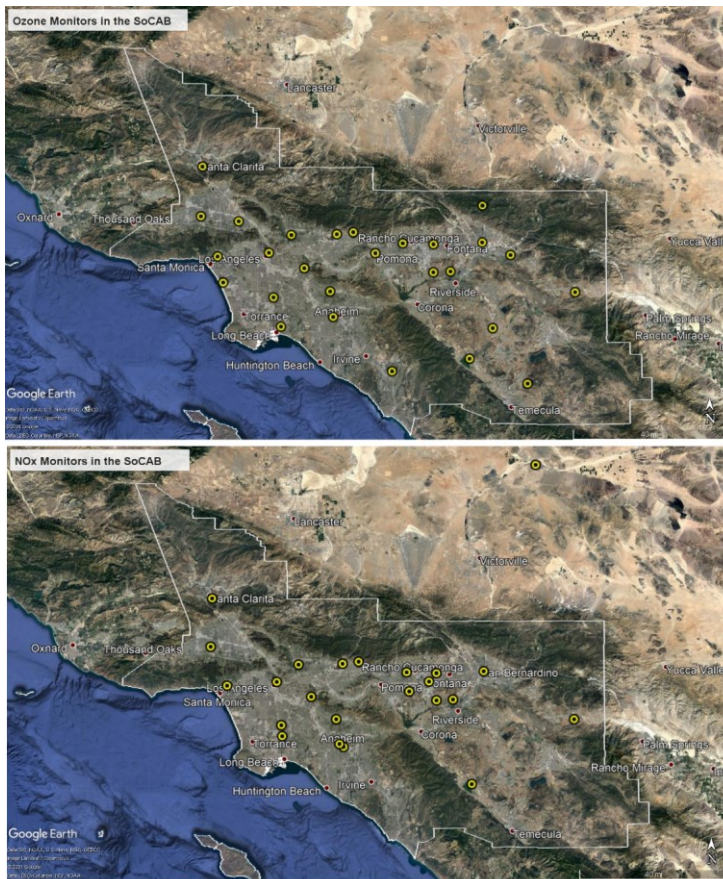
Figure 1. Maps of SoCAB surface O₃ and NO₂ monitors (top and bottom, respectively). The outline of the SoCAB boundary is shown as a white polygon.
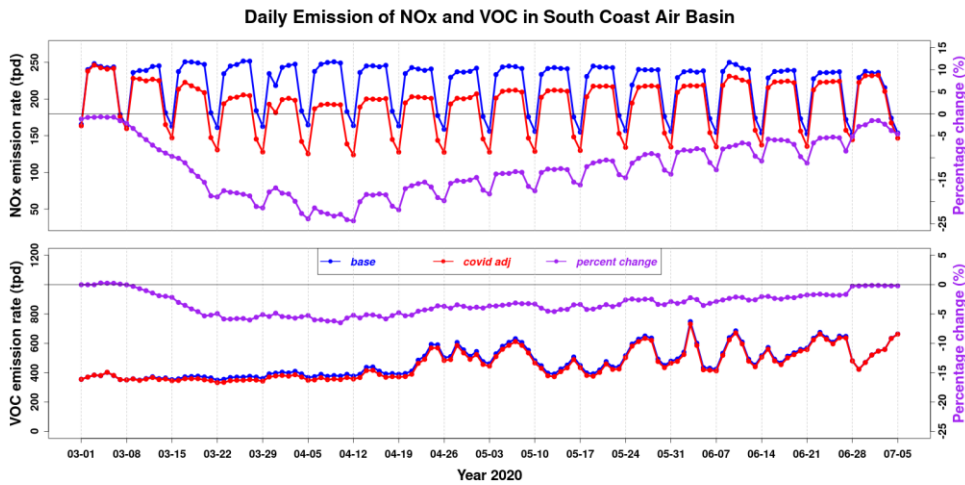
Figure 2. Daily total emissions of NOx and VOC in South Coast Air Basin. Blue lines are for baseline emissions and red lines are for COVID19 adjusted emissions. Purple lines are for the percentage changes of NO$_x$ and VOC due to COVID19 adjustment: (COV19 adjusted – baseline)/baseline. Vertical grey dash lines correspond to Sundays.
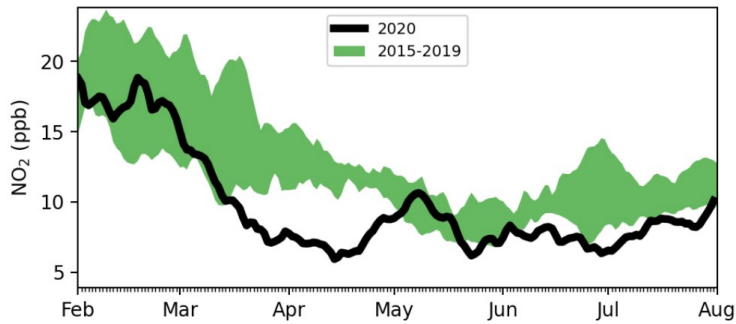
Figure 3. SoCAB pollutant concentrations for 2020 (black line) and for 2015 – 2019 (green shading). Data is averaged over 21 sites that contain data throughout the time period.
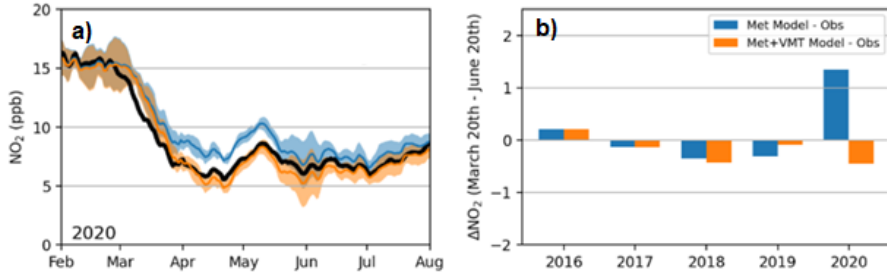
Figure 4. (a) Observed NO₂ (black) and predictions of daily NO₂ based on non-VMT variables (blue line). Uncertainty estimates are derived from the model-observation difference for the years on which the non-VMT model is trained (narrow envelope means the model performed well on the training data for that time of year). The model with VMT is shown (orange). Data has 21-day smoothing applied. (b) The average difference between the models and the observations for March 20th to June 20th for each year (models are trained on 2016-2019 data).
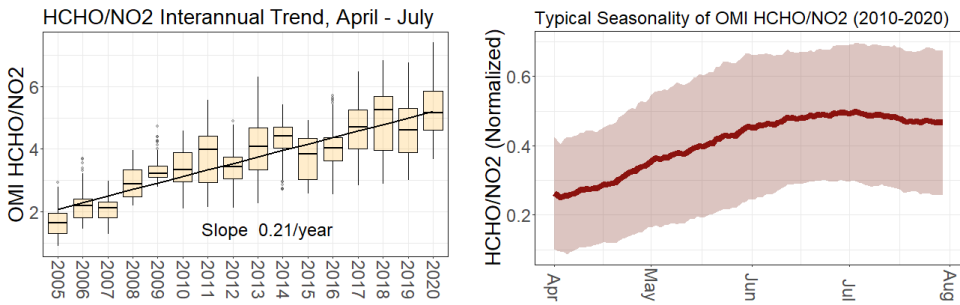
Figure 5. (Left) Interannual trend of OMI HCHO/NO₂ averaged over the SoCAB. Data are filtered to include the April – July period of each year. A linear fit is applied to the data. (Right) Typical seasonality of OMI HCHO/NO₂ averaged over the SoCAB. Data have been normalized to the range for each year.

Basin-average OMI HCHO/NO2, Binned by Basin-highest MDA8
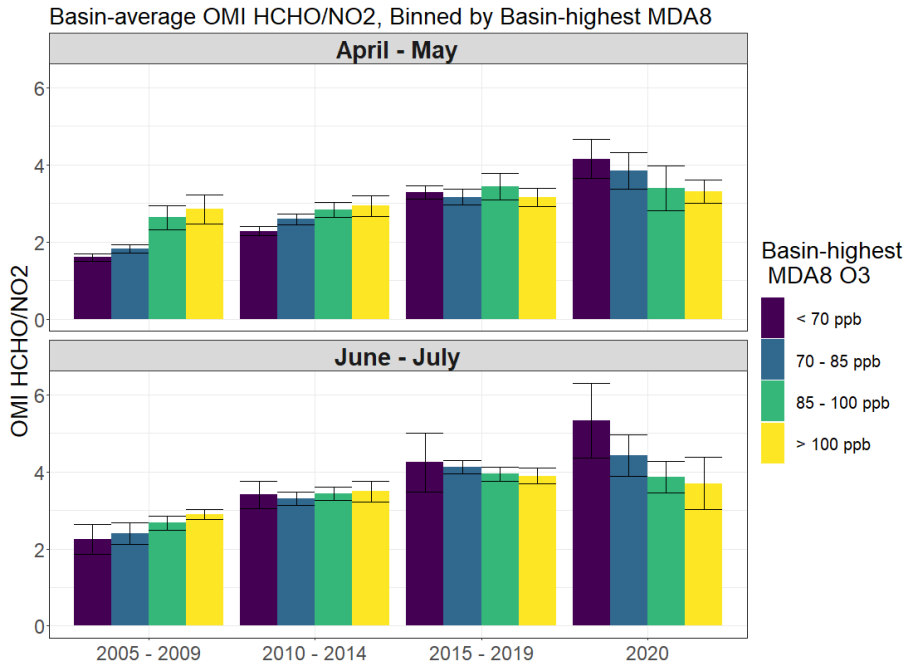
Figure 6. Time series of basin-average OMI HCHO/NO₂ ratios. Data are binned every five years, and colored by the basin-highest MDA8 observed on each day. Each bar represents the mean ± one standard deviation. The top panel shows data from Spring (April – May), and the bottom panel shows data from Summer (June – July).

Weekend/Weekday Effect over the Past Fifteen Years
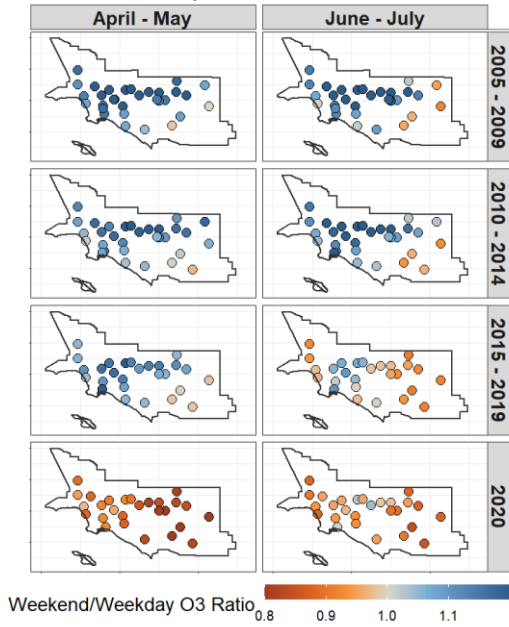
Figure 7. Time series of WE/WD O₃ ratios at SoCAB monitoring sites. Rows represent averages over five-year bins, and columns represent temporal bins for Spring (April – May) and Summer (June – July).
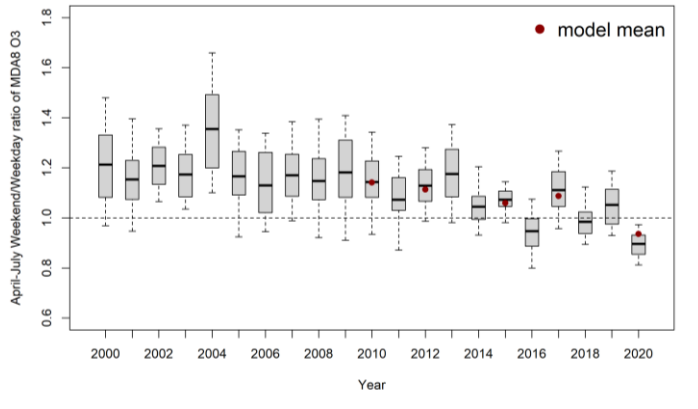
Figure 8. Boxplot: observed April-July WE/WD ratios of MDA8 O₃ at South Coast monitoring sites. The solid lines in each box are the mean ratios of all the sites. Red dot: modeled mean ratios.

615
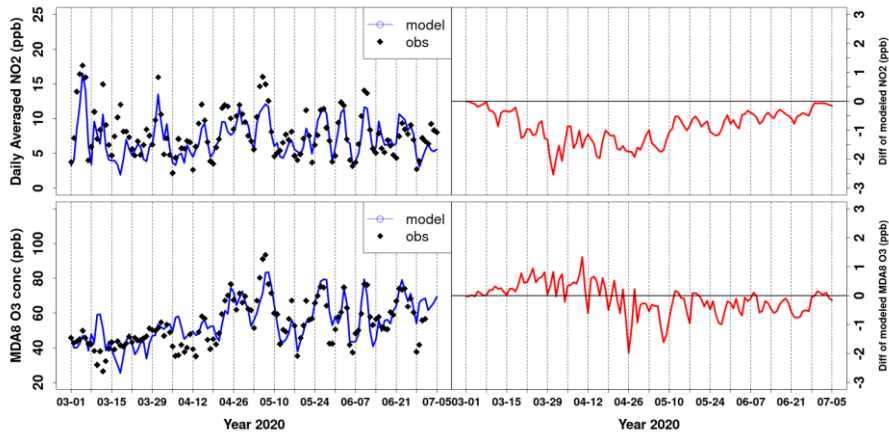
Figure 9. Left top: time series plots of daily averaged NO₂ concentrations in South Coast Air Basin from model and observation. Right top panel: time series plots of daily averaged NO₂ difference between the two sets of model simulations (model with COVID-19 adjusted emission inventory – model with baseline emission inventory). Left bottom panel: time series plots of daily maximum averaged 8-hour ozone concentrations in South Coast Air Basin from model and observation. Right bottom panel: time series plots

620 **of MDA8 O$_3$ difference between the two sets of model simulations (model with covid19 adjust emission inventory – model with baseline emission inventory).**